

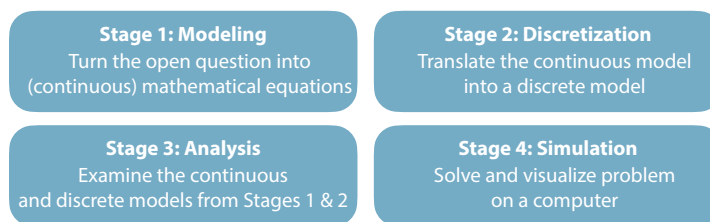
1.5 Perovskite Models, Finite Volume Methods, and Painless Simulation

Dilara Abdel, Patricio Farrell, Jürgen Fuhrmann, and Petr Vágner

The four stages of turning crystal ions into math

In 2019, perovskite solar cells (PSCs) beat classical silicon solar cells. At least in terms of efficiency. With a sunlight-current conversion rate of over 25%, the novel PSCs can match the well-known light blue solar cells which cover roofs all over Germany. Although PSCs continue performing better and better, they do not last very long – the perovskite material degrades too fast. How can we improve PSC efficiency and simultaneously prevent their degradation?

Answering such a question – just as many other scientific open problems at the Weierstrass institute – involves at least four different stages, namely



Guided by this real-life question for perovskites as well as related charge transport problems, all four stages will be highlighted in the following article. But before we turn to the math, we will briefly explain the physical principles of semiconductors, solar cells, and PSCs.

In general, a semiconductor is a solid that conducts electric current better than an insulator but worse than a metal. The atoms in solids are densely packed, which creates a conduction band – a new space for electrons through which they can travel. Only the atom's outermost, valence electrons can enter the conduction band, and only if they are given an additional energy – the so-called *band-gap energy*. In the case of metals, the band-gap energy is negligible, whereas it is considerably large for insulators. The band gap of semiconductors lies between the two. Hence, where can an electron in a semiconductor get the energy to enter the conduction band? There are three main sources of energy: thermal, mechanical, and radiative. We will focus on a particular source of the radiation – photons emitted by the sun, summarized in a generation process denoted by G_{ph} .

Roughly speaking, the core of a PSC consists of three parts: positively-doped semiconductor, perovskite, and negatively-doped semiconductor; see Figure 3. The doping in the semiconductors – artificially implanted positive or negative ions – alters the preference for holes and electrons. Therefore, the positively-doped semiconductor attracts electrons, whereas the negatively-doped semiconductor attracts holes. In between them, the perovskite, being also a semiconductor, generates the conduction electrons and valence holes. However, on top of those electrons and holes,



Fig. 1: A raw perovskite crystal named after the Russian mineralogist Lev Perovski (1792–1856)
(c) K. Nash, CC-BY 3.0, wikipedia/Perovskit

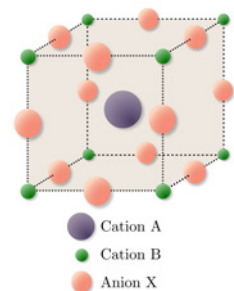


Fig. 2: Perovskite ideal unit cell ABX_3 . It consists of two cations A and B as well as an anion X; see [2]

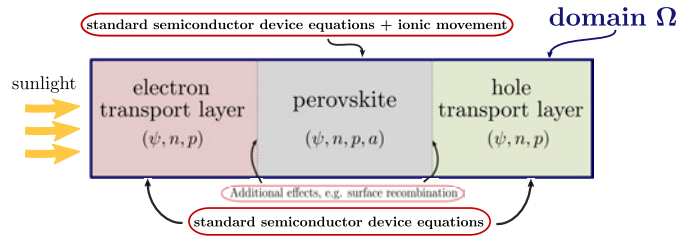


Fig. 3: A three-layer device with the relevant charge carrier densities per area (n for electrons, p for holes, and a for anion vacancies) as well as the electric potential ψ

the perovskite also contains charged vacancies, which are not fixed to the crystalline lattice, but migrate and affect the transport of the electrons and holes.

Perovskites form a class of crystalline solids with two cations and an anion – positively and negatively charged ions. Their idealized structure, visualized in Figure 2, is equivalent to the structure of a mineral with the same name discovered in the late 19th century. In reality, crystal defects occur that dynamically appear and reappear. They leave void spaces, called *vacancies*, within the crystal. For example, an ion next to a defect-caused vacancy can take advantage of the void space and occupy it, leaving a vacancy in its formerly occupied place. Even though the perovskites are solids, their microscopic behavior is similar to quicksands. This permanently changing crystalline structure affects the conduction electrons and valence holes like a dynamic doping, and it is not enough to consider only electrons and holes as carriers of charge. In perovskites, especially the movement of negatively charged anions influences the transport of charge that needs to be likewise captured by the model. We start with Stage 1 by turning the movement of crystal ions into mathematics.

Charge transport models for perovskites

Stage 1: Modeling

The interaction of electrons, holes, and electric potential in a semiconductor can be described by a system of partial differential equations introduced by van Roosbroeck in 1950; see [1]. We use this model to describe the doped transport layers; see Figure 3. As exposed in the Introduction, within PSCs, the moving anions in the perovskite influence the device behavior. To capture this influence, we describe the movement of anion vacancies – resulting in electrons n , holes p , and anion vacancies a as charge carriers. Their densities are denoted by n_α , $\alpha = n, p, a$. Within the perovskite layer, the semiconductor device equations (1a)–(1c) are extended by an additional equation (1d):

$$-\nabla \cdot (\epsilon_s \nabla \psi) = q(n_p - n_n + n_a - C), \quad (1a)$$

$$\partial_t n_n - \frac{1}{q} \nabla \cdot \mathbf{j}_n = G_{ph} - R(n_n, n_p), \quad (1b)$$

$$\partial_t n_p + \frac{1}{q} \nabla \cdot \mathbf{j}_p = G_{ph} - R(n_n, n_p), \quad (1c)$$

$$\partial_t n_a + \frac{1}{q} \nabla \cdot \mathbf{j}_a = 0, \quad (1d)$$

$$\mathbf{j}_a = -qz_a (D_a \nabla n_a + z_a \mu_a n_a \nabla \psi), \quad (1e)$$

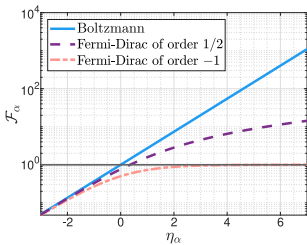


Fig. 4: Statistics functions

where ε_s denotes the dielectric permittivity, q the elementary charge, and C a background charge due to cation vacancies of the perovskite. The right-hand sides of (1b), (1c) are given by a generation G_{ph} , portraying the illumination by the sun, and present recombination processes summarized in R . Within the electric current \mathbf{j}_α , we have the charge number z_α , the diffusion coefficient D_α , and the mobility μ_α . The density of charge carriers can be related to the chemical potential η_α via [1]

$$n_\alpha = N_\alpha \mathcal{F}_\alpha(\eta_\alpha), \quad \alpha = n, p, a,$$

where N_α denotes the effective density of states, and \mathcal{F}_α a so-called *statistics function*. In many cases, we can choose the Fermi–Dirac integral of order one-half $F_{1/2}(\eta) = \frac{2}{\pi} \int_0^\infty \frac{\xi^{1/2}}{\exp(\xi - \eta) + 1} d\xi$ for electrons and holes. As opposed to $F_{1/2}$ and its usual Boltzmann approximation $F_{1/2}(\eta) \approx \exp(\eta)$ valid for small η , the statistics function $F_{-1}(\eta) = \frac{1}{\exp(-\eta) + 1}$ is always less than one; see Figure 4. Thus, it is well suited to the limited maximum concentration of the anion vacancies in perovskites.

As an extension, the charge transport model can be supplemented with further surface effects taking place between two different materials; see Figure 3.

Physics-preserving finite volume discretization

The continuous model (1) is analytically tractable only in special, simplified cases. Therefore, to simulate a realistic PSC, (1) will be approximated with a system of ordinary differential equations (ODEs), which we further solve using a computer. In particular, the ODEs are generated using the finite volume method [1] so that the system preserves physical properties of the PSC model. This method subdivides a computational domain $\Omega \subset \mathbb{R}^d, d = 1, 2, 3$, into a finite number N of control volumes ω_K , each associated with a node $\mathbf{x}_K \in \omega_K$; see Figure 5. For a given physical quantity, like, e.g., the electron density n_n , we use $n_{n,K}, n_{n,L}$, to denote its value at node $\mathbf{x}_K, \mathbf{x}_L$, respectively.

Furthermore, the system of partial differential equations is integrated over each control volume ω_K , using Gauss’s theorem and one-point quadrature rules. For example, the discrete counterpart of the electron mass balance (1b) reads

$$|\omega_K| \partial_t n_{n,K} - \frac{1}{q} \sum_{\omega_L \in \mathcal{N}(\omega_K)} |\partial\omega_K \cap \partial\omega_L| j_{n;K,L} = |\omega_K| (G_K - R(n_{n,K}, n_{p,K})),$$

where $\mathcal{N}(\omega_K)$ denotes the set of control volumes neighboring ω_K . Here, $j_{n;K,L}$ approximates the projected flux $\mathbf{j}_n \cdot \nu_{K,L}$ across the interface $\partial\omega_K \cap \partial\omega_L$, with normal vector $\nu_{K,L}$. This system of ODEs can be further discretized in time, e.g., by the implicit Euler method.

There are now several ways to adequately approximate the flux. For example, there exists the convenient excess chemical potential scheme [3, 4, 5], which extends the drift part in (1e) by the excess chemical potential, $\mu_\alpha^{ex} = \log \mathcal{F}_\alpha(\eta_\alpha) - \eta_\alpha$. The discrete flux reads

$$j_{\alpha;K,L} = -\frac{\mu_\alpha N_\alpha k_B T}{z_\alpha (x_L - x_K)} \left(B(-Q_{\alpha;K,L}) \mathcal{F}_\alpha(\eta_{\alpha;L}) - B(Q_{\alpha;K,L}) \mathcal{F}_\alpha(\eta_{\alpha;K}) \right), \quad (2)$$

Stages 2 & 3:
Discret. & Analysis

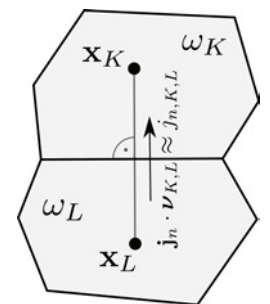


Fig. 5: Two neighboring control volumes

where $B(\xi) = \xi/(e^\xi - 1)$ is the Bernoulli function and

$$Q_{\alpha;K,L} = z_\alpha \frac{q(\psi_L - \psi_k)}{k_B T} + (\eta_{\alpha;L} - \eta_{\alpha,K}) - \log \frac{\mathcal{F}_\alpha(\eta_{\alpha;L})}{\mathcal{F}_\alpha(\eta_{\alpha;K})}.$$

Similar discretization schemes in the unipolar (single charged species with background charge) case and in the electrolyte case, where different charged quantities compete for the same space leading to a joint statistics distribution similar to the Fermi–Dirac integral of order -1 have been analyzed in [4, 5]. The discrete fluxes (2) lump the electrostatic force and the gradients of the excess chemical potential into a joint convective force. The resulting discrete system exactly conserves charge balances, both locally and globally. Moreover, the concentrations, given as the solution of the discrete system, will stay nonnegative during the evolution, and – in the case of statistics equal to Fermi–Dirac integral of order -1 – limited by the available amount of lattice sites. In addition, the discrete solutions relax to the steady state solution; see Figure 6. Results obtained for the special case of electrolytes with ion volume constraints [4, 5] suggest that also for the discrete perovskite model the relative free energy of the discrete solutions along a trajectory decays, and the solution of the discrete system is well defined, exists, and converges weakly to a solution of the continuous problem.

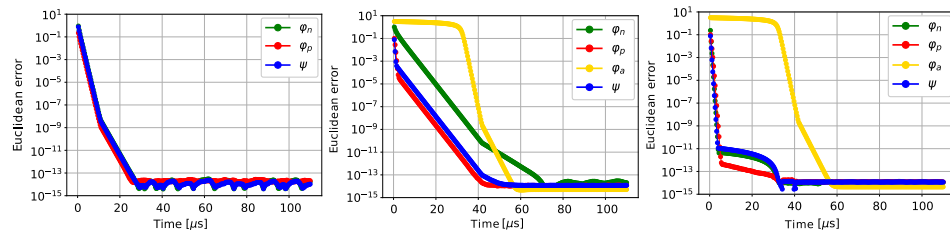


Fig. 6: Approach towards the steady state solution for a three layer PSC device. The error between transient and steady state solution for three configurations are depicted: without mobile ions, with mobile ions & with mobile ions and surface recombination as further surface effect; see Figure 3.

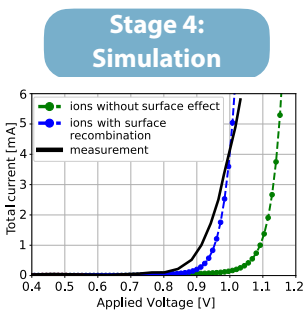


Fig. 7: Simulation of a forward scan protocol of a PSC device with additional surface effects

Painless simulation using automatic differentiation

In this section, we explain automatic differentiation and how we leverage it to solve the discrete systems. Solving a large system of nonlinear equations often relies on Newton’s method, which in each of its iterations requires the assembly of the Jacobi matrix – the matrix of partial derivatives – of the nonlinear operator. Calculating the partial derivatives and implementing them into program code is a straightforward but tedious and error-prone task which can be automated.

Forward mode automatic differentiation allows to evaluate a nonlinear function such that both its value and its derivative are obtained at once. A straightforward implementation is based on dual numbers \mathbb{D} defined by extending the set of real numbers \mathbb{R} . Similar to introducing the imaginary unit i with $i^2 = -1$ to define the complex numbers, one introduces a special number ε to define the set of dual numbers as $\mathbb{D} = \{a + b\varepsilon \mid a, b \in \mathbb{R}\}$. With positioning $\varepsilon^2 = 0$, the evaluation of a

polynomial $p(x) = \sum_{i=0}^n p_i x^i$ on a dual number $a + \varepsilon$ yields

$$p(a + \varepsilon) = \sum_{i=0}^n p_i a^i + \sum_{i=1}^n i p_i a^{i-1} \varepsilon = p(a) + p'(a) \varepsilon.$$

This fact can be generalized to differentiable functions of several variables and to multivariate dual numbers, allowing for the calculation of partial derivatives. The Julia computer language via the package `ForwardDiff.jl` provides an easily accessible implementation of dual number arithmetic helping to evaluate nonlinear functions along with their derivatives.

For implementing the Voronoi finite volume discretization as described above, we develop the Julia package `VoronoiFVM.jl`. It builds upon the experience available at WIAS on the implementation of the method [1]. It allows to describe discretizations of rather general nonlinear multiphysics reaction-diffusion-convection systems via reaction terms, flux functions like (2), and capacity terms. These constitutive functions are evaluated at discretization nodes and control volume interfaces using dual number arithmetic. The resulting local contributions are assembled into the residual vector of the discretized system and a sparse matrix representation of its Jacobi matrix. All computational results shown in this contribution and in references [2]–[6] have been obtained using this package.

Automatic calculation of Jacobians for discretized nonlinear systems of partial differential equations opens further computational possibilities. These include the utilization of efficient higher-order time discretization methods readily available in Julia via the package `DifferentialEquations.jl`. The Jacobi matrix evaluated at the steady state of a nonlinear system with an added frequency-dependent complex diagonal matrix can be used to obtain the phase shift and amplitude (related to the impedance) of the system response to a small periodic perturbation of this steady state. In [6], an implementation of a charge transport model for monocrytalline yttria-stabilized zirconia (YSZ)-based electrochemical cells in `VoronoiFVM.jl` has been used to fit measurements of cyclic voltammograms and impedance spectra to parameters of the model; see Figure 8.

We envision to include derivatives with respect to problem parameters into the automatic differentiation approach that should benefit parameter identification and bifurcation analysis. Foremost, the introduction of ion concentration limitation and further model improvements are aimed at supporting the qualitative understanding of the performance and degradation issues of PSCs. Efficient and flexible numerical implementations matching experimental measurements can verify and calibrate the model, allowing to optimize geometry and materials of PSCs in future research.

References

- [1] P. FARRELL, N. ROTUNDO, D.H. DOAN, M. KANTNER, J. FUHRMANN, TH. KOPRUCKI, *Chapter 50: Numerical Methods for Drift-Diffusion Models*, in: J. Piprek, ed., *Handbook of Optoelectronic Device Modeling and Simulation*, **2** (2017), CRC Press, Boca Raton, pp. 733–771.
- [2] D. ABDEL, P. VÁGNER, J. FUHRMANN, P. FARRELL, *Modelling charge transport in perovskite solar cells: Potential-based and limiting ion depletion*, *Electrochim. Acta*, **390** (2021), pp. 138696/1–138696/12.

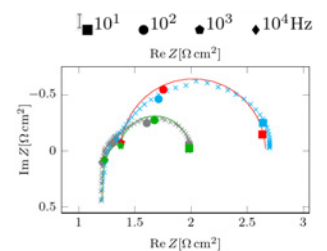


Fig. 8: Experimental result (markers) and fitted numerical simulation (solid lines) of an impedance spectrum of an YSZ device at 850 °C [6]

- [3] D. ABDEL, P. FARRELL, J. FUHRMANN, *Assessing the quality of the excess chemical potential flux scheme for degenerate semiconductor device simulation*, Opt. Quantum Electron., **53**:3 (2021), pp. 163/1–163/10.
- [4] C. CANCEËS, C. CHAINAIS-HILLAIRET, J. FUHRMANN, B. GAUDEUL, *A numerical-analysis-focused comparison of several finite volume schemes for a unipolar degenerate drift-diffusion model*, IMA J. Numer. Anal., **41**:1 (2021), pp. 271–314.
- [5] B. GAUDEUL, J. FUHRMANN, *Entropy and convergence analysis for two finite volume schemes for a Nernst–Planck–Poisson system with ion volume constraints*, Numer. Math. **151**:1 (2022), pp. 99–149.
- [6] V. MILOŠ, P. VÁGNER, D. BUDÁČ, M. CARDA, M. PAIDAR, J. FUHRMANN, K. BOUZEK, *Generalized Poisson–Nernst–Planck-based physical model of O₂ /LSMIYSZ electrode*, J. Electrochem. Soc., **169**:4 (2022), pp. 044505/1–044505/17.